Soft Matter

Check for updates

Fluid interface-assisted assembly of soft microgels: recent developments for structures beyond hexagonal packing

Déborah Feller [iD] and Matthias Karg [iD] *

Microgels adsorb to air/water and oil/water interfaces – a process driven by a significant reduction in interfacial tension. Depending on the available interface area per microgel, strong lateral deformation can be observed. Typically, hexagonally ordered structures appear spontaneously upon contact of the microgel shells. Transfer from the interface to solid substrates gives access to macroscopically sized microgel monolayers that are interesting for photonic and plasmonic studies as well as colloid-based lithography, for example. Significant efforts have been made to understand the phase behavior of microgels at different interfaces and to explore the available parameter space for achieving complex tessellations. In this review, we will discuss the most recent developments in the realization of microgel monolayers with structures beyond hexagonal packing.

1. Introduction

Thermoresponsive microgels were first prepared from *N*-isopropylacrylamide (NIPAM) in 1986 by Pelton and Chibante.[1] The authors used free-radical polymerizations performed above the lower critical solution temperature (LCST) of poly-NIPAM (PNIPAM), *i.e.* approximately 32 °C,[2,3] to obtain monodisperse,

*Institut für Physikalische Chemie I: Kolloide und Nanooptik, Heinrich-Heine-Universität Düsseldorf, Universitätsstr. 1, 40225 Düsseldorf, Germany.
E-mail: karg@hhu.de*

Déborah Feller studied Chemistry at the Heinrich-Heine-University Düsseldorf. During her studies, she was supported by the Deutschlandstipendium. She joined the group of Prof. Matthias Karg at the Institute of Physical Chemistry I: Colloids and Nanooptics in 2018 for her bachelor thesis and accomplished her master thesis in 2020. Currently, she is doing her PhD in the same group with the support of the AFR Individual

Déborah Feller

PhD grant from the Fonds National de la Recherche (FNR) Luxembourg. Her research focusses on the understanding and the control of self-assembling processes from Au-PNIPAM core–shell microgels at interfaces.

Matthias Karg studied Chemistry at the Technical University Berlin. He finished his PhD in Physical Chemistry working on stimuli-responsive microgels in the group of Prof. Thomas Hellweg in 2009. After a postdoctoral research stay as a fellow of the Alexander von Humboldt Foundation at the Nanoscience Laboratory of the University of Melbourne (Prof. Paul Mulvaney), he moved to the University of Bayreuth where he

Matthias Karg

became Juniorprofessor for Colloidal Systems in Physical Chemistry in 2012. Since 2016, he is a Full Professor at the Institute of Physical Chemistry I: Colloids and Nanooptics at the Heinrich-Heine-University Düsseldorf. His current research interests include general aspects of colloid and interfaces science with a special focus on the phase behavior of microgels in dense 2D and 3D packings.

submicrometer-sized microgels that varied in crosslinker and/or comonomer concentration. Later, in 1999 Zhang and Pelton demonstrated that PNIPAM microgels spontaneously adsorb to air/water interfaces leading to a significant reduction in interfacial tension.[4] They found that, rather independent of the crosslinker density, the interfacial tension is reduced to approximately 43 mN m^{-1}. Because of this property, microgels could be used to successfully stabilize emulsions.[5–8] However, recently Mehrabian et al. have shown by molecular dynamics simulations that the stabilization of emulsions by soft colloids may not have significant advantages compared to hard colloids.[9] In 2005, Ngai et al. studied the stabilization of octanol-in-water emulsions by poly-(NIPAM-co-methacrylic acid) copolymer microgels.[5] Very stable emulsions were obtained at room temperature and pH > 6, where the microgels were highly swollen and negatively charged. At low enough pH, where the net charge of the microgels was significantly reduced due to protonation of the carboxyl groups, destabilization and accumulation of the microgels in the oil phase was observed. Raising the temperature above the volume phase transition temperature (VPTT) resulted also in destabilized emulsions at pH < 8. Using cryo-scanning electron microscopy (cryo-SEM) Brugger et al. have investigated the microgel packing at oil/water interfaces. They observed pronounced differences compared to the behavior of solid particles in classical Pickering emulsions, i.e., interconnections between individual microgels at the interface were visualized. In 2012, Geisel et al. have gained first insights into the 3-dimensional structure of microgels adsorbed at oil/water interfaces.[10] Using freeze-fracture shadow casting cryo-SEM (FreSCa)[11] the authors showed that microgels laterally stretch at the interface with a particle diameter, d_i, that is significantly larger than the swollen-state hydrodynamic particle diameter in bulk, d_h. Furthermore, the authors found that the majority of the particle volume is immersed in the water phase. Inspired by these works, moving to flat interfaces and altering the area fraction of microgels turned out to be an exciting strategy to (1) study the phase behavior of soft, thermoresponsive microgels in 2-dimensional confinement, and (2) to get access to large area monolayer assemblies that can be transferred to solid substrates.[12–15] The thereby achievable substrate-supported microgel arrays were used for functional nanopatterning by (soft) nanosphere lithography.[13,16] Employing microgels that contained plasmonic, noble metal nanoparticles gave access to plasmonic surface coatings, where the optical response could be adjusted through the nanoparticle size and composition[17] or the interparticle distance controlled by the interfacial dimensions of the microgels.[18] Such monolayers of plasmonic hybrid microgels were used to study electromagnetic coupling in dependence of interparticle distance, in particular collective coupling scenarios due to plasmonic-diffractive coupling leading to surface lattice resonances.[19,20]

In recent years, new strategies to achieve microgel arrangements beyond hexagonal packing using fluid interface-assisted assembly were investigated. An important step in this direction is linking the molecular structure of microgels or soft particles in general to their morphology and collective behavior at interfaces.[21]

In this review, we summarize recent experimental developments in fluid interface-assisted (self-)assembly of microgels leading to monolayer structures beyond hexagonal packing. We mostly focus on works that were published within the past five years and that employ air/water or oil/water interfaces to restrict microgel assembly to 2-dimensional arrangements. This review is structured as follows: first, we introduce general aspects of microgels and their soft interactions. Then, we discuss the 2-dimensional arrangement and (self-)assembly of microgels at different interfaces. This is followed by a discussion on non-hexagonal structures that are obtained from single microgel monolayers. Then, assemblies from binary mixtures are introduced. As a last strategy we discuss structures achieved by multiple depositions onto the same substrate. We close this review with general conclusions and thoughts on future perspectives.

2. Microgels and soft interactions

Microgels are soft and deformable objects with dimensions in the colloidal regime, that is most commonly in the micron and submicron range.[22–24] They feature an internal gel-like structure consisting of chemically and/or physically crosslinked polymer chains.[25] Fig. 1a shows a schematic depiction of a microgel.

Under good solvent conditions, microgels can host large amounts of solvent which makes it difficult to classify them physically. The physical properties of swollen microgels range somewhere between macromolecules, surfactants and colloids.[23] Even when the solvent quality is reduced leading to collapse of microgels, they can contain significant amounts of solvent distinguishing them from classical rigid and non-deformable systems such as silica-, polystyrene- (PS) or polymethylmethacrylate-based (PMMA) colloids.[27,28] When microgels are composed of polymers that feature a LCST, with PNIPAM being the most widely known and studied example,[3] their volume can be manipulated simply by changing temperature.[29] This volume phase transition (VPT) behavior renders PNIPAM microgels as such an interesting system for fundamental research, for example to study phase transitions in dense packings, where the microgel volume fraction can be altered by temperature,[30] but also for applications in the field of sensing, drug delivery and as cell culture media.[31–34]

PNIPAM microgels are typically synthesized via free-radical precipitation polymerization leading to spherical microgels of low polydispersity. The dimensions of the microgels can be controlled in multiple ways, for example by using surfactants that lower the interfacial tension[35–37] or by using sequential polymerizations in a semi-batch fashion.[38] While microgels are typically synthesized in batch and semi-batch processes where upscaling is limited, using flow reactors was demonstrated to give access to larger quantities.[39] Typically, PNIPAM microgels are chemically crosslinked with N,N′-methylenebis(acrylamide) (BIS). Due to the higher reactivity of BIS compared to NIPAM,[40] the crosslinker density decreases from the center to the outside
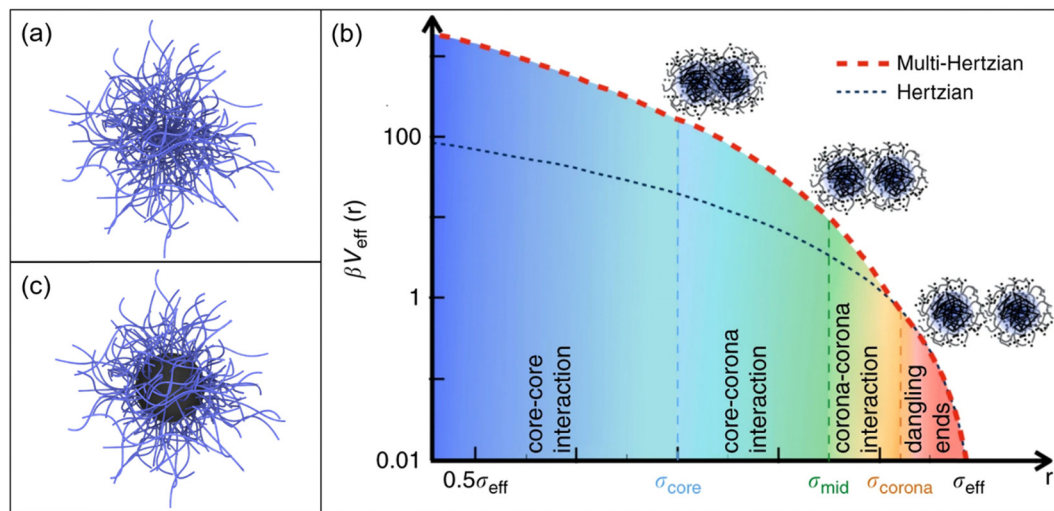
Fig. 1 (a) Schematic depiction of a microgel. (b) The multi-Hertzian model, describing best experimental data, is compared to the Hertzian model. The following length scales are considered in the model: below σ_{core} for core–core interactions, below σ_{mid} for core–shell interactions and at σ_{corona} for the heterogeneous nature of the outer shell. The y-axis is logarithmically scaled. Reproduced with permission from ref. 26. Copyright 2018 Nature Communications. (c) Schematic depiction of a core–shell microgel with a rigid core.

of the microgel.[41] In bulk dispersion this gradient leads to a 'core–shell' like structure, often described as fuzzy sphere. The higher crosslinked core is stiffer than the loosely crosslinked outer corona which directly influences the interaction between microgels. A soft Hertzian model that is often used to describe the interactions of microgels is not sufficient to describe such inhomogeneous, fuzzy sphere-like microgels.[42] Recently, Bergman *et al.* presented a multi-Hertzian (MH) model to describe the effective interactions between microgels in dependence of temperature and volume fraction.[26] In this model, the inner structure of microgels can be understood as a series of shells becoming less dense for greater distance to the center. The combined potential can thereby also quantify the strong core–corona and core–core interactions (Fig. 1b). Apart from the intrinsic core–shell-like structure of typical PNIPAM microgels, core–shell microgels with rigid organic or inorganic cores (see Fig. 1c) resemble a more extreme case where the rigid and non-deformable character of the core is combined with the soft, deformable character of the microgel shell.[43] One example are polystyrene-PNIPAM (PS-PNIPAM) core–shell-microgels that can be prepared in single-step or two-step polymerizations.[44–47] In contrast to the PNIPAM shell, the volume of the rigid PS cores cannot be changed by temperature – at least in aqueous environment. Furthermore, different inorganic nanoparticles such as silica or gold (Au), can be incorporated by seeded precipitation polymerization.[48–51] Interactions in core–shell microgel systems strongly depend on the shell-to-core size ratio. For example, microgels with rigid nanoparticle cores that are small with respect to the overall microgel size, behave basically identical as compared to microgels that do not feature a rigid core.[52] For small shell-to-core ratios, core–core interactions will become relevant, at least at high packing fractions. In any case, when it comes to interparticle interactions one needs to distinguish between mechanical stiffness, *i.e.* rigid as

in case of inorganic nanoparticles and soft as in case of (most) microgels[53] and interactions related to steric and/or electrostatic interactions. Electrostatic interactions are relevant to (most) rigid nanoparticles in aqueous environments and result in soft repulsive interactions at distances larger than the particle diameter – despite the particles themselves being rigid. Whether or not such repulsive interactions also impact the interaction in core–shell microgels has not been elucidated, yet.

When changing from bulk to interfaces, microgel–microgel interactions at fluid interfaces were successfully described by a simple Hertzian-like potential.[54,55] Nonetheless, this potential is not suitable to describe the formation of complex interfacial patterns that have been experimentally observed upon compression of microgel monolayers. Thus, a more complex potential has to be elaborated in the future. Furthermore, interactions become more complex when transferring microgels from the interface to a solid substrate. In this scenario, for example, capillary forces can become relevant during the transfer and will affect the interaction between microgels and consequently influence the assembly microstructure.[56] Here the Hertzian-like potential is not sufficient to explain the interactions between microgels.

Like many colloids, microgels and core–shell microgels strongly adsorb at air/water and oil/water interfaces. The significant reduction in interfacial tension upon adsorption does not only trap microgels at such interfaces but also causes a significant lateral deformation.[57] At the interface, soft microgels deform laterally to further decrease the free-energy of the interface. Thus, microgels occupy a larger area at the interface when compared to their bulk dimensions.[51] The degree of this stretching is limited by the bulk elasticity[58] and can be used as a measure for the softness.[53] With increasing crosslinker density, microgels become more rigid and stretching is less pronounced. Thus, the diameter at the fluid interfaces

approaches the diameter in bulk. The degree of deformation and the structural appearance are also influenced by the internal morphology, *e.g.* the fuzzy sphere structure of typical PNIPAM microgels. In that case, the shape of microgels at the interface is often referred to as fried-egg like.[59,60] The structure originates from the lower deformability of the highly cross-linked core compared to the loose shell.[40,41] This fried-egg like morphology is even more pronounced for core–shell microgels with rigid cores.[59] These structural aspects are not only relevant at fluid interfaces but also when these are used, for example, to coat solid substrates *via* transfer of microgel monolayers from the fluid interface. In the following, we will discuss some general aspects of interface-assisted self-assembly using liquid interfaces.

3. Liquid interface-assisted self-assembly

Drop casting of a dilute dispersion and subsequent drying is probably the easiest way to transfer microgels from dispersion to a solid substrate. While – at a first glance – it may be not intuitive, this process often involves assembly at the air/water interface of the droplet. Horigome and Suzuki studied the drying mechanism of PNIPAM microgel dispersions on poly-styrene substrates.[61] The authors were able to monitor the assembly of their rather large microgels *in situ* using optical video microscopy. It has been shown that, irrespective of the concentration in the range between 0.0005 and 0.01 wt%, microgels adsorb at the air/water interface of the aqueous droplet within a few minutes. During evaporation of the droplet, interparticle distances decreased and such the area fractions of microgels increased. Then, ordered structures were observed upon drying on the solid substrate. Importantly for concentrations of 0.0006 and 0.001 wt% homogeneous thin films with strong iridescent colors were obtained in contrast to the classical coffee ring effect often observed upon drop casting of dispersions of rigid particles. Later, Takizawa *et al.* investigated the drying process in dependence of the size, chemical structure and softness of the microgels.[62] The size of the microgels did not influence the adsorption at the air/water interface. In contrast, the softness and the surface activity of the microgels played an important role in the adsorption kinetics. The authors were able to optimize the conditions with respect to microgel architecture and drying conditions to achieve homogeneous thin films in very short time – much faster compared to conventional drying.

Similarly the group of Satapathy studied the self-assembly of PNIPAM microgels in the evaporation of sessile droplets.[63–66] By controlling the humidity, the authors were able to decelerate the evaporation.[64] Thus, the microgels had sufficient time to rearrange at the air/water interface. This led to highly ordered structures upon complete evaporation on solid substrates. Furthermore, the influence of the microgel softness on the obtained structures was investigated.[65] By increasing the soft-ness and controlling the humidity, the coffee ring effect could be minimized. Additionally, the authors managed to arrange binary mixtures of PNIPAM microgels into hexagonally ordered structures *via* evaporation self-assembly.[66] The deformability of the different sized microgels enabled the formation of a homo-genous monolayer. Nevertheless, the local order was found to depend on the position at the interface of the drop, meaning that the order in the middle of the drop could differ from positions more on the outside. While these examples nicely illustrate how adsorption at liquid interfaces and softness of microgels influence deposition on substrates, it remains diffi-cult to control the interface of the drop in terms of surface pressure and available area for the microgels. Furthermore, the size of the area on the solid substrate to be coated by microgels is limited by the dimensions of the sessile drop. Thus, it remains challenging to prepare cm^2 to m^2 thin films with high degrees of order and homogeneity independent of the position on the substrate.

Similar limitations are given for spin-coating. In this process potentially the adsorption to liquid interfaces prior to the final deposition step on the substrate also plays a crucial role for the final assembly structure. Nevertheless, for example, Schmidt *et al.* were able to prepare homogeneous thermoresponsive surface coatings by spin-coating of poly(NIPAM-*co*-acrylic acid) microgels.[67] Densely packed monolayers were obtained as studied by atomic force microscopy (AFM). Following this, Burmistrova *et al.* analyzed the packing density of poly-(NIPAM-*co*-acrylic acid) microgels in dependence of rotation speed, concentration and pH of the microgel dispersion.[68] Particle densities on the substrate increased with decreasing rotation speed, decreasing concentration and increasing pH. Thus, it is possible to adjust the amount of adsorbed microgels at the solid surface by controlling these three parameters. Jaber *et al.* used spin-coating to produce substrate-supported mono-layers of Au–PNIPAM core–shell microgels. Upon removal of the PNIPAM shells by heat treatment monolayers of non-close packed gold nanoparticles (initial cores) were achieved.[69]

The limitations in accessible assembly dimensions and control over microgel packing fractions can be overcome by changing to flat liquid interfaces as exemplarily shown in Fig. 2. Probably the most common way to assemble molecules, colloids and microgels at flat liquid interfaces is by using a Langmuir trough. Fig. 2a–c show photographs of a monolayer of Au–PNIPAM core–shell microgels at the air/water interface in a Langmuir trough. The barriers of the trough are open in (a) and more closed in (b). Due to the decrease of the available space, interparticle distances are reduced, resulting in a color change of the monolayer at the interface from light pink to light blue. In this example, the interparticle spacing is on the order of the visible wavelength causing the iridescent colors of the monolayer. When looking from a different angle at the inter-face, the iridescence can be observed more clearly (Fig. 2c).

Alternatively to using a Langmuir trough, floating mono-layers of microgels can be prepared in simple vessels like a crystallization dish.[18] Using different volumes of microgel dispersion that are injected to the interface or changing the concentration of the microgels from the spreading dispersion
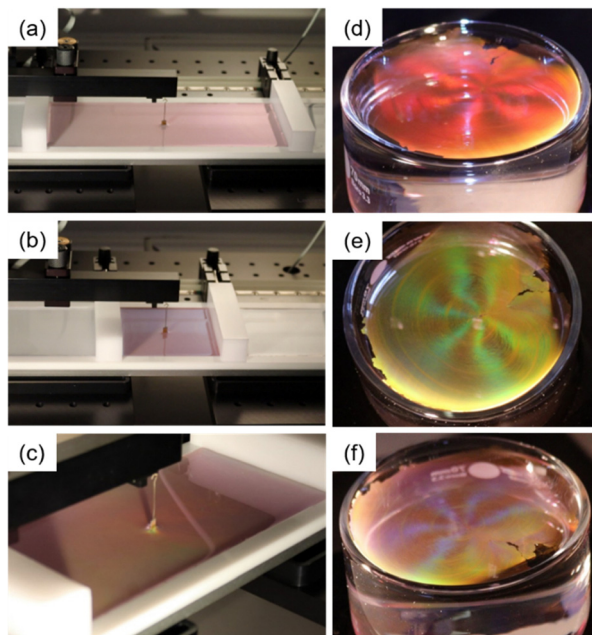
Fig. 2 Monolayers formed by Au–PNIPAM core–shell microgels at the air/water interface in (a–c) a Langmuir trough and in (d–e) a crystallization dish. (a) and (b) show the same monolayer at different compressions. The color of the monolayer changes from light pink to light blue. (c) shows the same monolayer as in the state of (b) but the photograph was taken from a different perspective. The iridescence of the arranged particles can be seen. (d)–(f) are photographs of the same monolayer in a crystallization dish taken from different angles, showing the angle-dependent iridescence of a monolayer at the air/water interface.

that typically involves a volatile, polar solvent like ethanol, allow control over the packing fraction – at least to some extent.[19] This is exemplarily demonstrated in Fig. 2d–f. The angle-dependent coloration of the monolayer at the air/water interface, from red to yellowish green to blueish violet, is the result of the hexagonal arrangement of the microgels with rather large domain sizes and interparticle spacings on the order of the visible wavelength.[70,71]

Studying microgels and their assemblies at fluid interfaces *in situ* is challenging due to the movement and often submicron size of microgels and is therefore not yet fully explored. Recently, two groups managed to investigate the 3-dimensional shape of microgels at the interface with different experimental techniques. Vialetto *et al.* investigated PNIPAM microgels at the oil/water interface by *in situ* AFM.[72] The authors could reconstruct the 3-dimensional shape of the microgels at the interface by recording AFM images, both, from the oil and the water side. They also studied the effects of the oil phase, the inner structure of the microgel and temperature on the conformation of the microgels. The authors could clearly see a change in microgel shape depending on the aforementioned parameters. Similarly, Bochenek *et al.* investigated the influence of temperature and inner morphology on the structural appearance of microgels at air/water interfaces using neutron reflectrometry.[73] The authors compared monolayers of microgels with 5 mol% crosslinker and ultra-low crosslinked (ULC) microgels. For both systems, an increase in temperature only affected the part of the

microgel dispersed in the water phase, but not the part in the air phase. The higher crosslinked core of "standard" microgels was found to be located in the air phase resulting in a contact angle of a few degrees. By contrast, the ULC microgels formed only a flat polymer layer comparable to linear polymer chains.

These findings in combination with earlier results from Zielinska *et al.* who used neutron reflectivity measurements to study the absorption kinetics, amount of absorbed material and resulting structure of microgels at air/water interfaces provide important insights into the behavior of microgels at fluid interfaces – studied *in situ*.[74,75] These insights will also become relevant when control of the microgel microstructure is desired.

Most often such microstructures are studied ex-situ upon transfer to solid substrates. Transfer of the monolayers from the liquid interface onto a solid substrate can be performed in different ways, mostly depending on the hydrophobicity of the substrate of interest. For example, Volk *et al.* used a hydrophilic glass substrate immersed in the bulk phase (water), moved the substrate under a freely floating monolayer and then used withdrawal of the substrate at a shallow angle through the monolayer for microgel deposition.[18] By this, it was possible to obtain hexagonally ordered monolayers with long-range order and excellent homogeneity. When assembled in a Langmuir trough depositions onto solid substrates are often realized in a more controlled fashion by a dip coater (Langmuir–Blodgett, Langmuir–Schäfer deposition). Here, it is also possible to transfer the monolayers from the liquid interface to a solid substrate during continuous compression. This will be further discussed in the next section.

3.1 Structural control *via* surface pressure

A simple, yet powerful way to alter the microstructural arrangement and interparticle distances in monolayers of microgels at fluid interfaces is *via* changing the accessible interface area using a Langmuir trough setup.[76] Typically, the trough area is defined by the position of two movable barriers. Through these barriers the interfacial area is uniaxially manipulated. With more specialized setups also radially symmetric manipulations of the interfacial area become possible.[77]

Already a simple compression experiment on microgels (poly(NIPAM-*co*-methacrylic acid) in a standard Langmuir trough reveals a complex phase behavior.[12] At low compression at water/*n*-hexane interfaces, such purely polymeric microgels spread to a maximum with large interparticle distances forming a gas-like phase for sufficiently low packing fractions. By increasing the compression, microgels arranged into a crystalline phase with hexagonal order and shell–shell contacts. From this point on the response to further compression strongly depends on the softness of the objects. The softer the shell, the more the microgels can be compressed until a phase transition occurs.[78] An isostructural phase transition with two defined length scales was observed upon further reduction of the available surface. Here a fraction of the microgels remained in shell–shell contact while another fraction was in "core–core" contact where "core" corresponds to

the inner, more densely crosslinked volume of the microgels. The appearance of this phase transition between two crystalline structures is strongly influenced by the inner structure and the size of the microgels.[13,78] Further compression increased the fraction of hexagonally ordered microgels in "core–core" contact until a dense monolayer remained. In this dense state, interparticle distances were smaller than the microgel size in bulk. According to Rey et al., the isostructural phase transition could not be detected for microgels with low crosslinking.[78] These microgels strongly deformed at fluid interfaces and defects of five- and seven-fold symmetries were observed. Similarly, Ciarella et al. studied the influence of microgel softness and architecture on the assembly behavior at fluid interfaces using experimental and theoretical results.[21] With a new coarse-grained simulation using augmented potentials the authors could account for the interfacial architecture and the phase behavior during reduction of the available surface area. Through this the authors could determine different multibody interactions occurring during the phase transitions. They achieved to differentiate between continuous, isostructural and heterostructural phase transitions. The continuous transition occured mostly for loosely crosslinked microgels as these exhibit a convex interaction potential. In contrast, core–shell microgels with a uniformly crosslinked shell, exhibited two internal length scales and mostly isostructural transitions were found. The shells of these microgels collapsed simultaneously and isotropically upon compression. The heterostructural transition was found for core–shell microgels with a non-uniformly crosslinked shell exhibiting two internal length scales. Here, phases like chains disturb the transition from non-close packed to close-packed hexagonal phases. The anisotropical collapsing of the shell causes this transition.

Such examples show that the softness and inner architecture strongly affects the phase behavior of microgels at interfaces. This becomes evident when further increasing the stiffness of the "core" of microgels, for example. This was studied by Rauh et al. using silica–PNIPAM core–shell microgels with different shell thicknesses.[59] Compression isotherms were recorded at water/n-hexane interfaces and the microstructure of the monolayer was linked to the respective surface pressure (see Fig. 3a). Similar to the work of Rey et al.[12] microstructural analysis was performed by continuously transferring the monolayer from the liquid interface to a solid substrate during the compression followed by ex situ analysis. At very high compressions above 25 mN m^{-1}, clustering of the microgels with "core–core" contact could be observed as shown in Fig. 3a-(i). At low compressions (in the range of a few mN m^{-1}), however, a distinct difference to the behavior of purely polymeric microgels was observed. Here, non-close packed hexagonal arrangements of the microgels with shell–shell contact were found as shown in Fig. 3a-(ii). The incorporation of a rigid, non-deformable core in the microgels lead to local deformations of the fluid interface. Such deformations influenced the arrangement already at low packing fractions due to attractive capillary interactions.[51,59] Thus, for these core–shell microgels clusters were already found at low area fractions and the

microgels did not form a homogenous monolayer.[14,51] This clustering depends on the shell-to-core size ratio but also on the shell architecture.[79] The thinner the shell for a given core size, the earlier the microgels will cluster during the compression.[59]

More recently Fernandez-Rodriguez et al. focused on the regime of low surface pressures in more detail.[56] The authors studied PNIPAM microgels with different crosslinker densities and different hydrodynamic diameters in bulk. The internal morphology of these microgels, i.e. the crosslinking and its distribution was varied through the monomer feeding in the respective polymerizations. At surface pressures close to 0 mN m^{-1}, rectangular arrangements were found for all systems as shown in Fig. 3b. The corresponding FFTs of the presented real space images exhibit each a clear four-fold symmetry and higher order peaks confirming the long-range order of the monolayers. The observed rectangular arrangements were discussed to be the result of an equilibrium between steric repulsion from the microgels and the attractive quadrupolar capillary interactions at the interface. The structures changed to the conventional hexagonal arrangement when the surface pressure was increased during the compression, starting at approximately 1 mN m^{-1}. Furthermore, the authors have applied the rectangularly arranged microgel monolayers for soft colloidal lithography applications. The monolayers were used as soft masks to prepare vertically aligned silicon nanowires via metal-assisted chemical wet etching and dry etching based on conventional deep reactive ion exchange.

Since PNIPAM microgels are temperature sensitive which allows for tuning of the microgel volume fraction in bulk aqueous dispersion by simply changing temperature, the question arises whether similar effects occur at fluid interfaces. Interestingly, Bochenek et al. could show that the temperature sensitivity is mostly lost at such interfaces and changes are only observed in microgel dimensions perpendicular to the interface.[80,81] In this example the lateral stretching in the interface driven by interfacial tension was the dominating effect influencing the arrangement and interaction of microgels.

Compressing monolayers of soft and deformable microgels and thereby controlling the surface pressure is a powerful way to study the phase behavior and interactions at liquid interfaces and to manipulate the spatial arrangement. In the following section we will address how the structural complexity can be even further increased by using binary assemblies.

3.2 Structural control via surface pressure: binary assemblies

A relatively simple way to extend structural complexity in colloidal monolayers is the combination of colloids of different sizes and/or different mechanical properties. In 2017, Rey et al. analyzed the anisotropic assembly of a mixture of isotropic hard and soft particles at the air/water interface during compression.[82] The authors mixed large PS particles ($d = 1.5$ μm) with an excess of small PNIPAM microgels ($d = 145$ nm) prior to the assembly at the interface in a Langmuir trough (see Fig. 4a). Due to attractive interactions between the microgels and the PS particles, the surface of the PS particles was covered by the soft
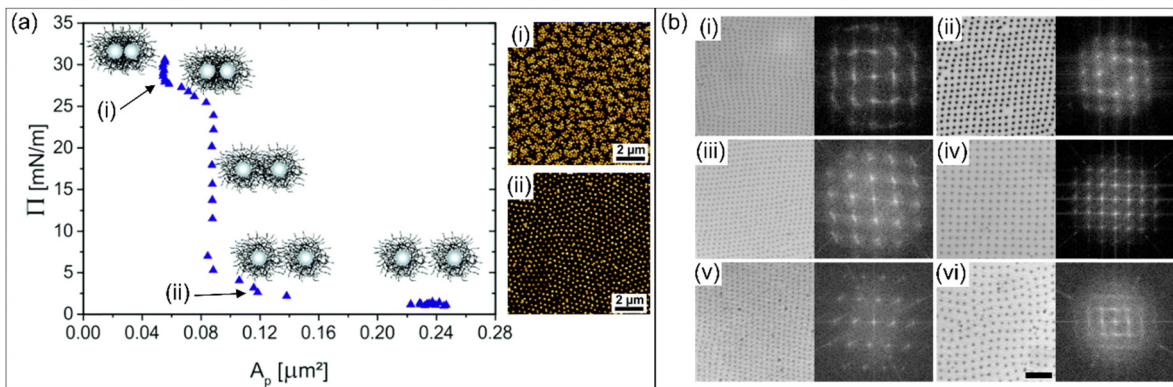
Fig. 3 (a) Compression isotherm for silica−PNIPAM core−shell microgels with two representative AFM images recorded from samples transferred to a solid substrate at different surface pressures. Adapted with permission from ref. 59. Copyright 2017 Royal Society of Chemistry. (b) Microscopy images of different microgels arranged in rectangular patterns on a silicon wafer and their corresponding FFTs. The FFTs are magnified three times and the scale bar corresponds to 5 μm. Reproduced with permission from ref. 56. Copyright 2021 Royal Society of Chemistry.

and deformable microgels. This deposition of the microgels resulted in effectively higher repulsion between the PS particles and prevented clustering due to capillary forces in the following assembly step. After deposition of the binary mixture at the air/water interface, a non-close packed hexagonally ordered structure could be observed at low compression. Here, the microgels covering the PS particles were just in contact without significant overlapping. During the increase in surface pressure upon reduction of the interfacial area by the barriers of the trough, the microgel shells started to overlap. Here, the observed microstructures changed to chain like and then to

square like arrangements, as shown in Fig. 4a top row. Upon further increase in packing fraction, a close packed hexagonally ordered structure with full overlap of microgel shells and PS particles in contact was obtained. The authors supported their experimental findings by Monte Carlo simulations of hard-core/soft-shell particles at different area fractions (Fig. 4a bottom row) and by minimum energy calculations. Interestingly, such structures were already theoretically predicted by the Jagla in 1998/99.[83,84] The calculations have shown that in order to obtain such complex structures, it is mandatory that the interaction potential of the particles displays two distinct
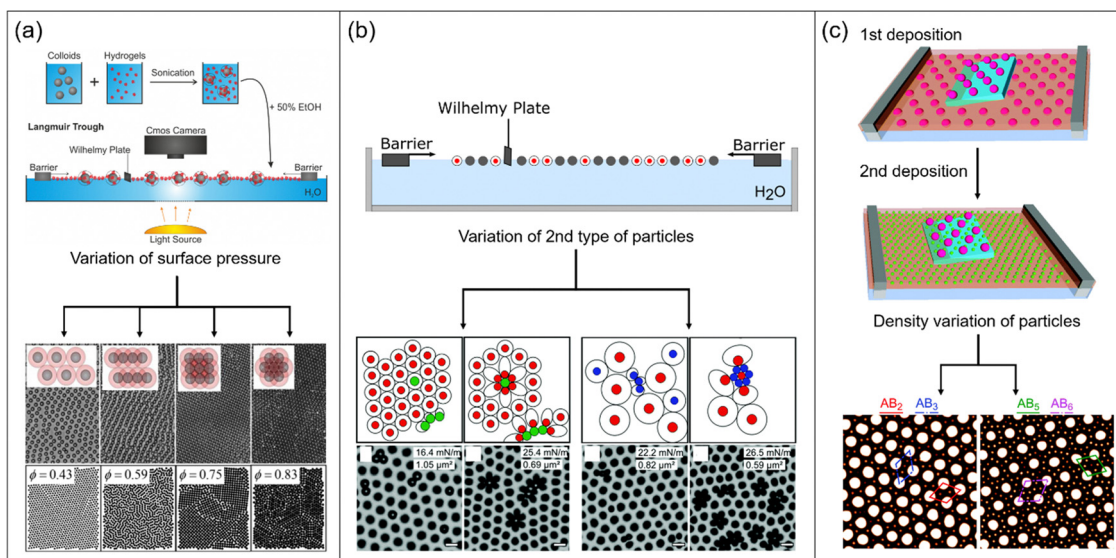

Fig. 4 (a) Schematic depiction of the binary assembly procedure. Mixtures of large PS particles and small PNIPAM microgels are applied to the air/water interface in a Langmuir trough. Depending on surface pressure, different phases can be observed experimentally (top row, microscopy images) and by Monte Carlo simulations (bottom row, images). Adapted with permission from ref. 82. Copyright 2017 American Chemical Society. (b) Schematic illustration of the assembly experiment in a Langmuir trough. By varying the type of the particles depicted as grey circles and the surface pressure, different structures are observed as schematically illustrated (top row) and experimentally evidenced by electron microscopy (bottom row). Adapted with permission from ref. 87. Copyright 2021 Royal Society of Chemistry. (c) Sketch of multiple deposition of large and small microgels, respectively. First, large microgels are transferred from the water/n-hexane interface to a silicon substrate. Second, small microgels are transferred onto the same silicon substrate. By varying the packing fraction of the particles, different structures can be observed in the AFM images. Adapted with permission from ref. 16. Copyright 2018 Royal Society of Chemistry.

length scales. Therefore, the potential is best described by the interplay of a hard sphere potential representing the core, here PS particles and a longer ranged soft repulsion shoulder representing the shell, here PNIPAM microgels. The anisotropic arrangements then present the minimum energy structure for the corresponding particle density. The group of Buzza completed the theoretical findings of Rey *et al.* by tuning different parameters like the soft shoulder profile, the density of the shell profile and the shell-to-core ratio.[85] They found additional structures such as honeycomb patterns and quasicrystals with 10- and 12-fold symmetry. The formation of quasicrystalline structures was also already predicted by Dotera *et al.* based on theoretical simulations using a simple core-shoulder profile.[86]

Using microgels with different mechanical properties, *i.e.* stiffness, Harrer *et al.* prepared non-hexagonal structures by interface-mediated assembly and subsequent transfer to solid substrates.[87] The authors applied two different mixtures of microgels at the air/water interface in a Langmuir trough and analyzed the resulting arrangements upon compression (see Fig. 4b). PNIPAM microgels with a crosslinker density of 2.5 mol% were present in both mixtures and only the second type of microgels was varied. These microgels are referred to as large microgels and are represented by red circles in Fig. 4b. For the first mixture, silica–PNIPAM core–shell microgels (5 mol% crosslinker density), represented by green circles, were added to an excess of large microgels. In the expanded state, the microgels and the core–shell microgels displayed similar interfacial sizes. Thus, the mixture formed a non-closed packed hexagonal structure at low compression (approximately 10 mN m^{-1} surface pressure). The core–shell microgels fitted perfectly in the lattice of the larger microgels. During compression starting at a surface pressure of approximately 15 mN m^{-1} a first phase transition was observed where neighboring core–shell microgels collapsed. Interestingly, in this regime neither neighboring microgels nor neighboring pairs of microgels and core–shell microgels collapsed (Fig. 4b left side). Mostly dimers and trimers of collapsed core–shell microgels were formed due to the excess of microgels and therefore the lower possibility of neighboring core–shell particles. Flower-like arrangements were observed, when the surface pressure was increased above 22 mN m^{-1}. Here, all the core–shell microgels and directly neighboring microgels collapsed. Thus, a monolayer of flower-like assemblies surrounded by a hexagonal lattice of non-collapsed microgels was observed. When the surface pressure is further increased (above approximately 27 mN m^{-1}), a third phase transition was observed. Here, all remaining microgels collapsed. Similar experiments were performed with another binary mixture. The second mixture consisted of the large microgels (as before) and PNIPAM microgels with a crosslinker density of 5 mol%, referred to as small microgels and represented by blue circles in Fig. 4b (bottom right). For a mixing ratio of 10 to 1, all microgels were in shell-shell contact at low compressions. The microgels displayed different interfacial diameters in this expanded state. When the surface pressure was increased above 19 mN m^{-1}, the beginning of a phase transition was observed. Neighboring small microgels

started to collapse into core–core contacts. The small microgels assembled to form a hexagonal close-packed arrangement. Interestingly, small microgels that were only in contact with large ones were not affected by the collapsing and still remained swollen. While the compression was pursued above a surface pressure of 25 mN m^{-1}, only large microgels in contact with small microgels started to collapse into core–core contacts. At this point, the aforementioned flower-like structure could be observed again (see Fig. 4b bottom right). The authors explained that the flower-like structure was stable and no rearrangement of the microgels could be observed. A hexagonally close-packed lattice was found, when the surface pressure was increased above 28 mN m^{-1}. At this value, all microgels collapsed to core–core contacts. This example nicely illustrates the interplay between mechanical properties, surface pressure and structural arrangements.

While in the work of Harrer *et al.* binary mixtures of microgels were directly applied to the interface, Fernandez-Rodriguez *et al.* prepared binary structures of differently sized particles *via* multiple deposition.[16] In Fig. 4c, the process of this double deposition at water/*n*-hexane interfaces in a Langmuir trough is schematically shown. For the first deposition, PNIPAM microgels (d_h = 940 nm) were compressed from 1 to 10 mN m^{-1} surface pressure. Simultaneously a silicon wafer was continuously withdrawn to transfer the monolayer from the interface to a solid substrate. Due to the increase of surface pressure, the interparticle distance between the microgels continuously decreased in the course of monolayer transfer. Onto the first hexagonally ordered layer of large microgels, a second layer of small PNIPAM microgels (d_h = 426 nm) was transferred during continuous compression from 1 to 22 mN m^{-1}. Thus, a binary monolayer was prepared with microgel gradients from low coverage to high coverage. At low surface pressure and high interparticle distance between the large microgels, five to six small microgels were found in the interstices (Fig. 4c right). When the large microgels were arranged with smaller interparticle distances at high compression, only two to three small microgels were found at the interstices. Thus, depending on the surface pressure, the authors could control the number of small microgels in the interstices of hexagonally arranged large microgels. While the examples of this section showed how assembly structures can be manipulated by introducing a second particle species that differs in size and/or stiffness, we will discuss structures from multiple depositions using single types of isotropic microgels in the next section.

3.3 Structural control *via* surface pressure: multiple deposition

A simple, yet powerful procedure to achieve more complex array structures from fluid interface-mediated self-assembly of microgels is the sequential deposition of more than one monolayer onto the same solid substrate. For example, Honold *et al.* used the sequential double deposition of freely floating microgel monolayers from air/water interfaces to solid substrates to prepare honeycomb structures.[88] In this work, two hexagonally

ordered monolayers were transferred consecutively onto the same glass substrate. Microgels in the monolayer transferred in the second deposition step settle in the voids in between neighboring microgels from the first deposited layer leading to a honeycomb structure. Importantly, due to their soft and deformable character and the significant reduction in size during drying, the resulting honeycomb arrays were real 2-dimensional structures rather than AB-type multilayers that would result from similar assemblies of hard spheres. The authors have also demonstrated that this approach is suitable to achieve binary plasmonic lattices by using core–shell microgels with gold nanoparticle cores (Au–PNIPAM) for the first and with silver nanoparticle cores (Ag–PNIPAM) for the second deposition. Volk *et al.* have shown that the drying conditions upon deposition on solid substrates play a crucial role in such

self-tessellating assemblies.[89,90] Followed by the deposition of the first, hexagonally ordered monolayer to the solid substrate, slow drying of the second monolayer resulted in honeycomb lattices whereas fast drying lead to Moiré-type lattices (see Fig. 5a). Supported by Brownian dynamics (BD) simulations, it was shown that the mobility of the particles in the second on top of the first monolayer (prior to complete drying) is crucial for the structure formation.[89]

Recently, Grillo *et al.* extended the variety of structures made from PNIPAM microgels by preparing non-regular tessellations such as herringbone superlattices. They used a double deposition process from monolayers prepared in a Langmuir trough at the water/n-hexane interface, as shown in Fig. 5b.[54] A first layer of microgels was transferred to a solid substrate during compression to form a hexagonally ordered monolayer with a
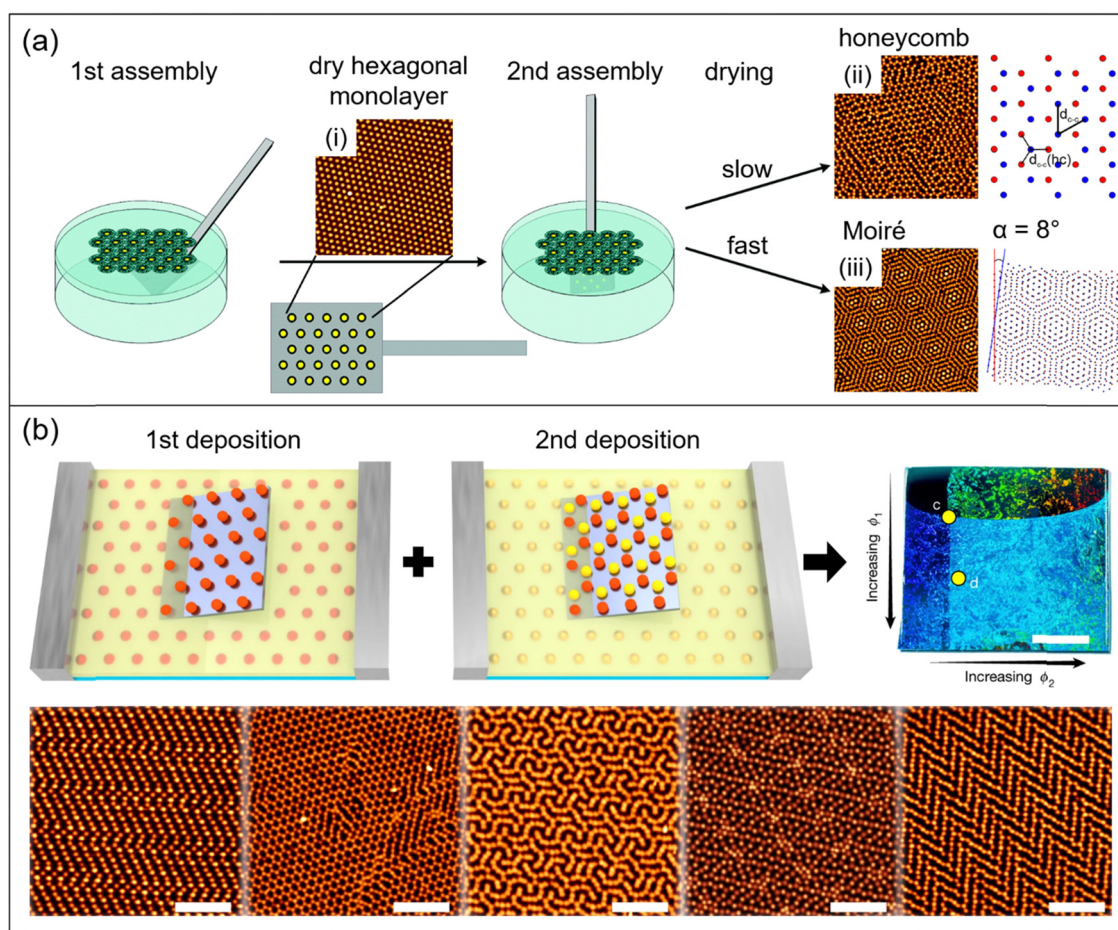

Fig. 5 (a) Schematic illustration of a multiple deposition process to form microgel monolayers with honeycomb and Moiré structures. From left to right: First, core−shell microgels are self-assembled at the air/water interface. After the first transfer to a glass substrate and consecutive drying a hexagonally ordered monolayer (immobile) is obtained (i). In the second assembly step another monolayer is transferred from the air/water interface onto the same substrate carrying the first monolayer. Depending on the drying conditions, either honeycomb (ii) or Moiré (iii) structures are obtained. Adapted with permission from ref. 89. Copyright 2019 Owner Societies. Adapted with permission from ref. 90. Copyright 2021 Wiley-VCH GmbH. (b) From top left to top right: schematic depiction of a double deposition process with PNIPAM microgels assembled at water/*n*-hexane interfaces using a Langmuir trough. The first monolayer is transferred to a silicon substrate during compression (1st deposition). In a second step, the substrate is turned by 90° and then a second monolayer is transferred onto the substrate during compression (2nd deposition). Photograph of the resulting structures on the silicon substrate with increasing packing fraction of the first monolayer from top to bottom and increasing packing fraction of the second monolayer from left to right (scale bar corresponds to 0.5 cm). From bottom left to bottom right: AFM images of structures with different packing fractions of first and second monolayer (scale bars correspond to 5 μm). Adapted with permission from ref. 54. Copyright 2020 Nature.

gradient in packing fraction. The substrate was then rotated by 90° prior to the second deposition to get two orthogonal gradients of packing fractions. The second monolayer was applied on top of the first one which acts as a template. Microgels from the first monolayer were immobile on the substrate, while microgels from the second deposition were mobile and could rearrange in the interstices of the first one. Thus, rectangular and honeycomb lattices, as well as interlocking-S structures, hexagonal and herringbone superlattices were prepared in this way. The authors confirmed that the structures are thermodynamically stable ones using molecular dynamics (MD) simulations. The observed structures were related to short-range repulsive interactions.

4. Conclusion and perspectives

Soft microgels adsorb to oil/water and air/water interfaces forming monolayers or submonolayers depending on the packing fraction. The cross-sectional area per microgel at such interfaces depends on the degree of compression, *i.e.* the applied surface pressure. The maximum achievable compression however is linked to the elasticity of the microgels. In the last years two distinct length scales were frequently observed in microgel monolayers, one corresponding to microgels in shell–shell contact and the other one corresponding to core–core contact. At intermediate surface pressures, these two length scales lead to clusters of microgels with different interparticle distances but the overall same hexagonal arrangement. Using assemblies of binary mixtures of particles that differ in size and/or softness is a powerful strategy to create unusual surface patterns. These structures can be controlled by the applied surface pressure capitalizing on the different response of the different particles. Phase transition were found to be linked to the softness of the microgels. This softness can be synthetically tailored by the internal morphology of the microgels by the degree of crosslinking and/or the introduction of rigid, non-deformable cores. In the last years, combinations of rather rigid homogeneous spheres, classical microgels with different degrees of crosslinking as well as core–shell microgels with rigid cores and soft microgel shells were used in interface-mediated self-assembly at different interfaces. Another approach to tailor microstructures in microgel monolayers is the repeated deposition of monolayers from oil/water or air/water interfaces onto the same solid substrate. This can lead to, for example, honeycomb and Moiré type structures that cover macroscopic areas with homogeneous packing fractions. Adding compression during the simultaneous transfer onto solid substrates has been demonstrated to lead to even more complex tessellations such as interlocking-S and herringbone structures.

Although first experiments have demonstrated that microgel softness plays a crucial role for the phase behavior at liquid interfaces, the correlation between internal structure and composition with respect to softness relevant at liquid interfaces has been barely studied. This gap is most likely related to the different behavior at liquid interfaces as compared to bulk,

where microgels are isotropic over a broad range of concentration and the softness of microgels can be easily quantified through rather standard experiments.[53] The role of shell architecture and the resulting interaction potential in complex interfacial self-assembly has been recently demonstrated by using core–shell particles with a linear, brush-like polymer shell rather than crosslinked microgels.[79] In the future, exploring the role of electrostatic interactions, for example in core–shell microgels with strongly charged cores, might be interesting for exploring an even broader parameter space and getting access to more complex interactions and potentially microstructures.

Another challenge in the field is related to the often exhaustive microstructure analysis based on microscopic techniques (mostly scanning electron and atomic force microscopy) applied to monolayers after transfer onto a solid substrate, *i.e. ex situ*. *In situ* studies on the monolayer behavior at liquid interface are scarce and could booster the knowledge gain in the field. Since the role of substrate hydrophobicity on the deposition behavior on solid substrates has been studied on the individual microgel level,[91] changing the surface chemistry of the substrate may provoke significant changes in microstructure. Quantifying this and understanding of drying effects requires the direct comparison between *in situ* and *ex situ* analysis of monolayer prior to and after transfer from liquid interfaces. The investigation of the impact of chemical and/or topological heterogeneities of substrates used for transfer is another interesting direction that has barely been touched in the field. Apart from generating a more general fundamental understanding of how soft colloids or colloidal like objects behave at liquid interfaces and upon transfer to a solid substrate, exploring structural complexity in liquid interface-assisted assembly will booster materials development, for example in sensing, photonics and even plasmonics.

Conflicts of interest

There are no conflicts to declare.

Acknowledgements

References

1 R. H. Pelton and P. Chibante, *Colloids Surf.*, 1986, **20**, 247–256.
2 M. Heskins and J. E. Guillet, *J. Macromol. Sci., Part A: Pure Appl.Chem.*, 1968, **2**, 1441–1455.

3 A. Halperin, M. Kroger and F. M. Winnik, *Angew. Chem., Int. Ed.*, 2015, **54**, 15342–15367.

4 J. Zhang and R. Pelton, *Langmuir*, 1999, **15**, 8032–8036.

5 T. Ngai, S. H. Behrens and H. Auweter, *Chem. Commun.*, 2005, 331–333.

6 T. Ngai, H. Auweter and S. H. Behrens, *Macromolecules*, 2006, **39**, 8171–8177.

7 M. Destribats, V. Lapeyre, M. Wolfs, E. Sellier, F. Leal-Calderon, V. Ravaine and V. Schmitt, *Soft Matter*, 2011, **7**, 7689–7698.

8 B. Brugger and W. Richtering, *Langmuir*, 2008, **24**, 7769–7777.

9 H. Mehrabian, J. H. Snoeijer and J. Harting, *Soft Matter*, 2020, **16**, 8655–8666.

10 K. Geisel, L. Isa and W. Richtering, *Langmuir*, 2012, **28**, 15770–15776.

11 L. Isa, F. Lucas, R. Wepf and E. Reimhult, *Nat. Commun.*, 2011, **2**, 438.

12 M. Rey, M. Á. Fernández-Rodríguez, M. Steinacher, L. Scheidegger, K. Geisel, W. Richtering, T. M. Squires and L. Isa, *Soft Matter*, 2016, **12**, 3545–3557.

13 L. Scheidegger, M. A. Fernandez-Rodriguez, K. Geisel, M. Zanini, R. Elnathan, W. Richtering and L. Isa, *Phys. Chem. Chem. Phys.*, 2017, **19**, 8671–8680.

14 N. Vogel, C. Fernández-López, J. Pérez-Juste, L. M. Liz-Marzán, K. Landfester and C. K. Weiss, *Langmuir*, 2012, **28**, 8985–8993.

15 C. Picard, P. Garrigue, M.-C. Tatry, V. Lapeyre, S. Ravaine, V. Schmitt and V. Ravaine, *Langmuir*, 2017, **33**, 7968–7981.

16 M. Á. Fernández-Rodríguez, R. Elnathan, R. Ditcovski, F. Grillo, G. M. Conley, F. Timpu, A. Rauh, K. Geisel, T. Ellenbogen, R. Grange, F. Scheffold, M. Karg, W. Richtering, N. H. Voelcker and L. Isa, *Nanoscale*, 2018, **10**, 22189–22195.

17 T. Honold, K. Volk, A. Rauh, J. P. S. Fitzgerald and M. Karg, *J. Mater. Chem. C*, 2015, **3**, 11449–11457.

18 K. Volk, J. P. S. Fitzgerald, M. Retsch and M. Karg, *Adv. Mater.*, 2015, **27**, 7332–7337.

19 E. Ponomareva, K. Volk, P. Mulvaney and M. Karg, *Langmuir*, 2020, **36**, 13601–13612.

20 K. Volk, J. P. S. Fitzgerald, P. Ruckdeschel, M. Retsch, T. A. F. König and M. Karg, *Adv. Opt. Mater.*, 2017, **5**, 1600971.

21 S. Ciarella, M. Rey, J. Harrer, N. Holstein, M. Ickler, H. Löwen, N. Vogel and L. M. C. Janssen, *Langmuir*, 2021, **37**, 5364–5375.

22 M. Karg, A. Pich, T. Hellweg, T. Hoare, L. A. Lyon, J. J. Crassous, D. Suzuki, R. A. Gumerov, S. Schneider, I. I. Potemkin and W. Richtering, *Langmuir*, 2019, **35**, 6231–6255.

23 F. A. Plamper and W. Richtering, *Acc. Chem. Res.*, 2017, **50**, 131–140.

24 J. Brijitta and P. Schurtenberger, *Curr. Opin. Colloid Interface Sci.*, 2019, **40**, 87–103.

25 W. Richtering and B. R. Saunders, *Soft Matter*, 2014, **10**, 3695–3702.

26 M. J. Bergman, N. Gnan, M. Obiols-Rabasa, J.-M. Meijer, L. Rovigatti, E. Zaccarelli and P. Schurtenberger, *Nat. Commun.*, 2018, **9**, 5039.

27 E. Ponomareva, B. Tadgell, M. Hildebrandt, M. Krüsmann, S. Prévost, P. Mulvaney and M. Karg, *Soft Matter*, 2022, **18**, 807–825.

28 S. Sbeih, P. S. Mohanty, M. R. Morrow and A. Yethiraj, *J. Colloid Interface Sci.*, 2019, **552**, 781–793.

29 C. Wu, S. Zhou, S. C. F. Au-yeung and S. Jiang, *Die Angew. Makromol. Chem.*, 1996, **240**, 123–136.

30 D. Lapkin, N. Mukharamova, D. Assalauova, S. Dubinina, J. Stellhorn, F. Westermeier, S. Lazarev, M. Sprung, M. Karg, I. A. Vartanyants and J. M. Meijer, *Soft Matter*, 2022, **18**, 1591–1602.

31 Y. F. Gao, X. Li and M. J. Serpe, *RSC Adv.*, 2015, **5**, 44074–44087.

32 Q. M. Zhang, W. D. Wang, Y. Q. Su, E. J. M. Hensen and M. J. Serpe, *Chem. Mater.*, 2016, **28**, 259–265.

33 M. Dirksen, C. Dargel, L. Meier, T. Brandel and T. Hellweg, *Colloid Polym. Sci.*, 2020, **298**, 505–518.

34 S. Schmidt, M. Zeiser, T. Hellweg, C. Duschl, A. Fery and H. Möhwald, *Adv. Funct. Mater.*, 2010, **20**, 3235–3243.

35 K. von Nessen, M. Karg and T. Hellweg, *Polymer*, 2013, **54**, 5499–5510.

36 M. Andersson and S. L. Maunu, *J. Polym. Sci., Part B: Polym. Phys.*, 2006, **44**, 3305–3314.

37 B. Wedel, T. Brandel, J. Bookhold and T. Hellweg, *ACS Omega*, 2017, **2**, 84–90.

38 M. Dulle, S. Jaber, S. Rosenfeldt, A. Radulescu, S. Förster, P. Mulvaney and M. Karg, *Phys. Chem. Chem. Phys.*, 2015, **17**, 1354–1367.

39 H. J. M. Wolff, M. Kather, H. Breisig, W. Richtering, A. Pich and M. Wessling, *ACS Appl. Mater. Interfaces*, 2018, **10**, 24799–24806.

40 X. Wu, R. H. Pelton, A. E. Hamielec, D. R. Woods and W. McPhee, *Colloid Polym. Sci.*, 1994, **272**, 467–477.

41 M. Stieger, W. Richtering, J. S. Pedersen and P. Lindner, *J. Chem. Phys.*, 2004, **120**, 6197–6206.

42 P. S. Mohanty, D. Paloli, J. J. Crassous, E. Zaccarelli and P. Schurtenberger, *J. Chem. Phys.*, 2014, **140**, 094901.

43 M. Karg, *Macromol. Chem. Phys.*, 2016, **217**, 242–255.

44 N. Dingenouts, C. Norhausen and M. Ballauff, *Macromolecules*, 1998, **31**, 8912–8917.

45 N. Dingenouts, S. Seelenmeyer, I. Deike, S. Rosenfeldt, M. Ballauff, P. Lindner and T. Narayanan, *Phys. Chem. Chem. Phys.*, 2001, **3**, 1169–1174.

46 T. Hellweg, C. D. Dewhurst, E. Brückner, K. Kratz and W. Eimer, *Colloid Polym. Sci.*, 2000, **278**, 972–978.

47 T. Hellweg, C. D. Dewhurst, W. Eimer and K. Kratz, *Langmuir*, 2004, **20**, 4330–4335.

48 M. Karg, I. Pastoriza-Santos, L. M. Liz-Marzán and T. Hellweg, *ChemPhysChem*, 2006, **7**, 2298–2301.

49 A. Rauh, T. Honold and M. Karg, *Colloid Polym. Sci.*, 2016, **294**, 37–47.

50 R. Contreras-Cáceres, J. Pacifico, I. Pastoriza-Santos, J. Pérez-Juste, A. Fernández-Barbero and L. M. Liz-Marzán, *Adv. Funct. Mater.*, 2009, **19**, 3070–3076.

51 S. A. Vasudevan, A. Rauh, L. Barbera, M. Karg and L. Isa, *Langmuir*, 2018, **34**, 886–895.

52 A. Rauh, N. Carl, R. Schweins and M. Karg, *Langmuir*, 2018, **34**, 854–867.

53 A. Scotti, M. F. Schulte, C. G. Lopez, J. J. Crassous, S. Bochenek and W. Richtering, *Chem. Rev.*, 2022, **122**, 11675–11700.

54 F. Grillo, M. A. Fernandez-Rodriguez, M.-N. Antonopoulou, D. Gerber and L. Isa, *Nature*, 2020, **582**, 219–224.

55 F. Camerin, N. Gnan, J. Ruiz-Franco, A. Ninarello, L. Rovigatti and E. Zaccarelli, *Phys. Rev. X*, 2020, **10**, 031012.

56 M. A. Fernandez-Rodriguez, M.-N. Antonopoulou and L. Isa, *Soft Matter*, 2021, **17**, 335–340.

57 H. Minato, M. Murai, T. Watanabe, S. Matsui, M. Takizawa, T. Kureha and D. Suzuki, *Chem. Commun.*, 2018, **54**, 932–935.

58 R. W. Style, L. Isa and E. R. Dufresne, *Soft Matter*, 2015, **11**, 7412–7419.

59 A. Rauh, M. Rey, L. Barbera, M. Zanini, M. Karg and L. Isa, *Soft Matter*, 2017, **13**, 158–169.

60 A. Mourran, Y. Wu, R. A. Gumerov, A. A. Rudov, I. I. Potemkin, A. Pich and M. Möller, *Langmuir*, 2016, **32**, 723–730.

61 K. Horigome and D. Suzuki, *Langmuir*, 2012, **28**, 12962–12970.

62 M. Takizawa, Y. Sazuka, K. Horigome, Y. Sakurai, S. Matsui, H. Minato, T. Kureha and D. Suzuki, *Langmuir*, 2018, **34**, 4515–4525.

63 M. Mayarani, M. G. Basavaraj and D. K. Satapathy, *Nanoscale*, 2017, **9**, 18798–18803.

64 M. Mayarani, G. B. Madivala and K. S. Dillip, *J. Colloid Interface Sci.*, 2021, **583**, 683–691.

65 M. Jose, M. G. Basavaraj and D. K. Satapathy, *Soft Matter*, 2021, **17**, 7921–7931.

66 M. Jose, M. Mayarani, M. G. Basavaraj and D. K. Satapathy, *Phys. Chem. Chem. Phys.*, 2021, **23**, 7115–7124.

67 S. Schmidt, H. Motschmann, T. Hellweg and R. von Klitzing, *Polymer*, 2008, **49**, 749–756.

68 A. Burmistrova and R. von Klitzing, *J. Mater. Chem.*, 2010, **20**, 3502.

69 S. Jaber, M. Karg, A. Morfa and P. Mulvaney, *Phys. Chem. Chem. Phys.*, 2011, **13**, 5576.

70 C. D. Sorrell, M. C. D. Carter and M. J. Serpe, *ACS Appl. Mater. Interfaces*, 2011, **3**, 1140–1147.

71 C. D. Sorrell and M. J. Serpe, *Adv. Mater.*, 2011, **23**, 4088–4092.

72 J. Vialetto, S. N. Ramakrishna and L. Isa, 2022, arXiv:2204.09324.

73 S. Bochenek, F. Camerin, E. Zaccarelli, A. Maestro, M. M. Schmidt, W. Richtering and A. Scotti, *Nat. Commun.*, 2022, **13**, 3744.

74 K. Zielińska, H. Sun, R. A. Campbell, A. Zarbakhsh and M. Resmini, *Nanoscale*, 2016, **8**, 4951–4960.

75 K. Zielińska, R. A. Campbell, A. Zarbakhsh and M. Resmini, *Phys. Chem. Chem. Phys.*, 2017, **19**, 17173–17179.

76 K. Geisel, W. Richtering and L. Isa, *Soft Matter*, 2014, **10**, 7968–7976.

77 S. K. Kale, A. J. Cope, D. M. Goggin and J. R. Samaniuk, *J. Colloid Interface Sci.*, 2021, **582**, 1085–1098.

78 M. Rey, X. Hou, J. S. J. Tang and N. Vogel, *Soft Matter*, 2017, **13**, 8717–8727.

79 J. Menath, J. Eatson, R. Brilmayer, A. Andrieu-Brunsen, D. M. A. Buzza and N. Vogel, *Proc. Natl. Acad. Sci. U. S. A.*, 2021, **118**, e2113394118.

80 S. Bochenek, A. Scotti, W. Ogieglo, M. A. Fernandez-Rodriguez, M. F. Schulte, R. A. Gumerov, N. V. Bushuev, I. I. Potemkin, M. Wessling, L. Isa and W. Richtering, *Langmuir*, 2019, **35**, 16780–16792.

81 S. Bochenek, A. Scotti and W. Richtering, *Soft Matter*, 2021, **17**, 976–988.

82 M. Rey, A. D. Law, D. M. A. Buzza and N. Vogel, *J. Am. Chem. Soc.*, 2017, **139**, 17464–17473.

83 E. A. Jagla, *Phys. Rev. E: Stat. Phys., Plasmas, Fluids, Relat. Interdiscip. Top.*, 1998, **58**, 1478–1486.

84 E. A. Jagla, *J. Chem. Phys.*, 1999, **110**, 451–456.

85 W. R. C. Somerville, A. D. Law, M. Rey, N. Vogel, A. J. Archer and D. M. A. Buzza, *Soft Matter*, 2020, **16**, 3564–3573.

86 T. Dotera, T. Oshiro and P. Ziherl, *Nature*, 2014, **506**, 208–211.

87 J. Harrer, S. Ciarella, M. Rey, H. Löwen, L. M. C. Janssen and N. Vogel, *Soft Matter*, 2021, **17**, 4504–4516.

88 T. Honold, K. Volk, M. Retsch and M. Karg, *Colloids Surf., A*, 2016, **510**, 198–204.

89 K. Volk, F. Deißenbeck, S. Mandal, H. Löwen and M. Karg, *Phys. Chem. Chem. Phys.*, 2019, **21**, 19153–19162.

90 K. Volk, T. Honold, D. Feller and M. Karg, *Adv. Mater. Interfaces*, 2021, **8**, 2100317.

91 L. H. Alvarez, S. Eisold, R. A. Gumerov, M. Strauch, A. A. Rudov, P. Lenssen, D. Merhof, I. I. Potemkin, U. Simon and D. Wöll, *Nano Lett.*, 2019, **19**, 8862–8867.